Automated Type Identification and Size Measurement for Low-Voltage Metering Box Based on RGB-Depth Image

Pengyuan Liu[1], Xurong Jin[2*], Shaokui Yan[3], Tingting Hu[4], Yuanfeng Zhou[5], Ling He[6], Xiaomei Yang[7]
Marketing Service Center (Metrology Center), State Grid Ningxia Electric Power Co., Ltd, Yinchuan, China[1, 2, 3, 4, 5]
College of Biomedical Engineering, Sichuan University, Chengdu, China[6]
College of Electrical Engineering, Sichuan University, Chengdu 610065, China[7]

***Abstract*—The low-voltage metering box is a critical piece of equipment in the power supply system. The automated inspection of metering boxes is important in their production, transportation, installation, operation and maintenance. In this work, an automated type identification and size measurement method for low-voltage metering boxes based on RGB-D images is proposed. The critical components, including the door shell and window, connection terminal block, and metering compartment in the cabinet, are segmented first using the Mask-RCNN network. Then the proposed Sub-Region Closer-Neighbor algorithm is used to estimate the number of connection terminal blocks. Combined with the number of metering compartments, the type of metering box is classified. To refine the borders of the metering box components, an edge correction algorithm based on the Depth Difference (Dep-D) Constraint is presented. Finally, the automated size measurement is implemented based on the proposed Equal-Region Averaging algorithm. The experimental results show that the accuracies of the automated type identification and size measurement of the low-voltage metering box reach more than 92%.**

Keywords*—Low-voltage metering box; RGB-D image processing; automated size detection; automated type detection; inspection automation

I. INTRODUCTION

The low-voltage metering box is an important piece of electrical equipment in power systems. It is responsible for measuring and monitoring the electrical energy consumption of end-users, which are ordinary residents, factories or enterprises [1-2]. It plays a pivotal role in ensuring that the power supply in a building is well regulated and efficiently distributed.

The automated inspection of low-voltage metering boxes is important in their production, transportation, installation, operation and maintenance [3-4]. The type identification and structural size inspection are of significance for the safety and the long-term use of the low-voltage metering boxes [5-6]. The type and size inspection refers to the process of examining the structure, physical shape and size of critical components in a metering box [7-8]. The structure and size of these components should be consistent with the relevant standards and regulations to ensure the proper functioning of the metering boxes. The conforming structure and size are prerequisites for a reasonable, safe and reliable layout of components of the metering boxes. The inappropriate type and size may lead to equipment damage or electrocution accidents, which can reduce the service life of the metering boxes. The type and structural size inspection is essential to ensure the safe and accurate operation of the low-voltage metering boxes and improve the reliability of electrical systems.

The inspection is typically carried out by a qualified technician in accordance with established procedures and guidelines. The technician should check the exterior and interior of the low-voltage metering box, including the appearance, key components, markings, and size measurement, which is labor-intensive and time-consuming. The automated inspection is urgent for a low-voltage metering box [9-12]. To a certain extent, it can improve the management efficiency and extend its service life.

Machine vision and other computer technologies make the automation inspection of metering boxes possible. Wang et al. [13] designed an intelligent detection management system for the low-voltage metering cabinets to optimize the inspection process and im-prove the detection efficiency. Shen et al. [14] analyzed the failure mechanism of the metering boxes to further improve their production process. Xu et al. [15] and Weng et al. [16] introduced image-based intelligent monitoring for the low-voltage metering cabinets to guard against theft and facility damage. However, there has been little research about the automatic type identification and size measurement of the low-voltage metering boxes.

To improve the efficiency of industrial production, there have been some studies on the size measurement of workpieces based on image processing and recognition technology. Three common approaches for size measurement are the monocular vision method, the binocular vision method and the structured light method, which are described as follows. (1) The monocular vision method is a commonly used method that uses a single camera to capture a workpiece image and combined with prior knowledge to compute the actual size of the workpiece [17]. Li et al. [18] proposed an axial dimension detection method for a corrugated compensator based on the image recognition. Chen et al. [19] introduced the Canny edge detection and contour feature extraction algorithm to identify the outer diameter and wall thickness of pipes. Cheng et al. [20] applied the camera calibration to measure the key size of injection-modeled products. Yu et al. [21] took the actual height as a reference to calculate the sizes of key parts of the

human body. (2) The binocular vision method uses two images which are acquired from different angles, and the three-dimensional spatial location information of the object can be obtained based on the parallax principle. Xue et al. [22] used the Kinect sensors to identify the size and orientation of square box objects, which can be used in mobile robots handling. Liu et al. [23] achieved an on-site size measurement of large forgings based on binocular stereo-vision and forging scene geometry constraints. (3) The principle of the structured light method for size measurement is optical triangulation [24]. The surface of the object modulates the structured light, and the modulated light is captured by a charge-coupled device (CCD), which forms a two-dimensional distorted image [24]. The 3D coordinates and contour in-formation of the designated point could be obtained based on the distorted image and the location of the modulated light bars.

The automated measurement of the workpiece size based on machine vision generally consists of two steps. The first step is to extract an edge or edge feature points of the workpiece via image processing. Then the two-dimensional coordinates are mapped into 3D space by modeling or calculation to obtain the actual size of the workpiece. Different workpieces have different shapes and physical characteristics. Thus, the size measurement method should be designed based on the characteristics of the captured images. The workpiece size measurement approaches mentioned above almost all focused on the measurement of a single small part. It is not applicable for the external and internal size measurement of the low-voltage metering box.

The low-voltage metering boxes with direct connections are classified into four types: single-phase single-meter metering boxes, single-phase multi-meter metering boxes, three-phase single-meter metering boxes, and three-phase multi-meter metering boxes [25]. The phase of a metering box is determined by the number of connection terminal blocks. For a single-phase metering box, the number of connection terminal blocks is four while it is eight for a three-phase metering box. The meter of a metering box is determined by the number of the metering compartments. The accurate automated type identification of the metering boxes remains a difficult problem, due to the illumination, occlusion, and other problems. In particular, the baffle plate in front of the connection terminal blocks significantly affected the detection accuracy.

In this work, an automated type identification and size measurement method for low-voltage metering boxes based on RGB-D (red, green, blue, and depth) images is pro-posed. The critical components, including the door shell and window, metering compartment, and connection terminal block in the cabinet, are segmented first using the Mask-RCNN network. Then the proposed Sub-Region Closer-Neighbor algorithm is used to estimate the number of connection terminal blocks. Combined with the number of metering compartments, the type of the metering box is classified. To refine the border of the metering box components, the edge correction algorithm based on the Depth Difference (Dep-D) Constraint is presented. Finally, the automated size measurement is implemented based on the proposed Equal-Region Averaging algorithm.

The main contributions of this work are summarized as follows:

- The automated type identification and size measurement method for the low-voltage metering boxes is proposed, based on RGB-D image processing techniques.
- The Sub-Region Closer-Neighbour algorithm for the number estimation of connection terminal blocks is proposed. Based on the calculated number of connection terminal blocks and metering compartment, the type of a metering box is identified.
- For the automatically segmented contour of critical components, the edge correction algorithm is proposed based on the proposed Depth Difference (Dep-D) Constraint in the depth channel. Then, the automated size measurement is implemented based on the proposed Equal-Region Averaging algorithm.

The rest of this paper is organized as follows. Section II introduces the proposed automated type identification and size measurement algorithm for low-voltage metering boxes. Section III describes the dataset and the experimental results. Finally, the conclusions are presented in Section IV.

II. Proposed Automated Type Identification and Size Measurement Algorithm for Low-Voltage Metering Boxes

The low-voltage metering box is a critical component of numerous electrical systems, functioning to guarantee the secure and effective distribution of electrical power [26]. Specifically, this device is utilized to measure and monitor electrical energy consumption within residential, commercial, or industrial settings.

A low-voltage metering box includes two parts: the door shell and the metering cabinet. In the door shell, there are door windows. In the metering cabinet, there are incoming compartment, metering compartment, outgoing compartment, mounting plate, watt-hour meter plug, plug interference fit, plug clearance fit, connection terminal block, and wire. Specially, the sizes of three critical components are essential in the inspection of the low-voltage metering box, which are door shell, door window and metering compartment. The structure of a low-voltage metering box is illustrated in Fig. 1.

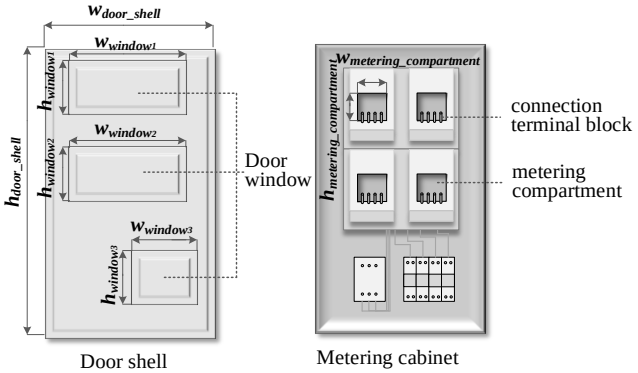

Fig. 1. Structure of a low-voltage metering box.

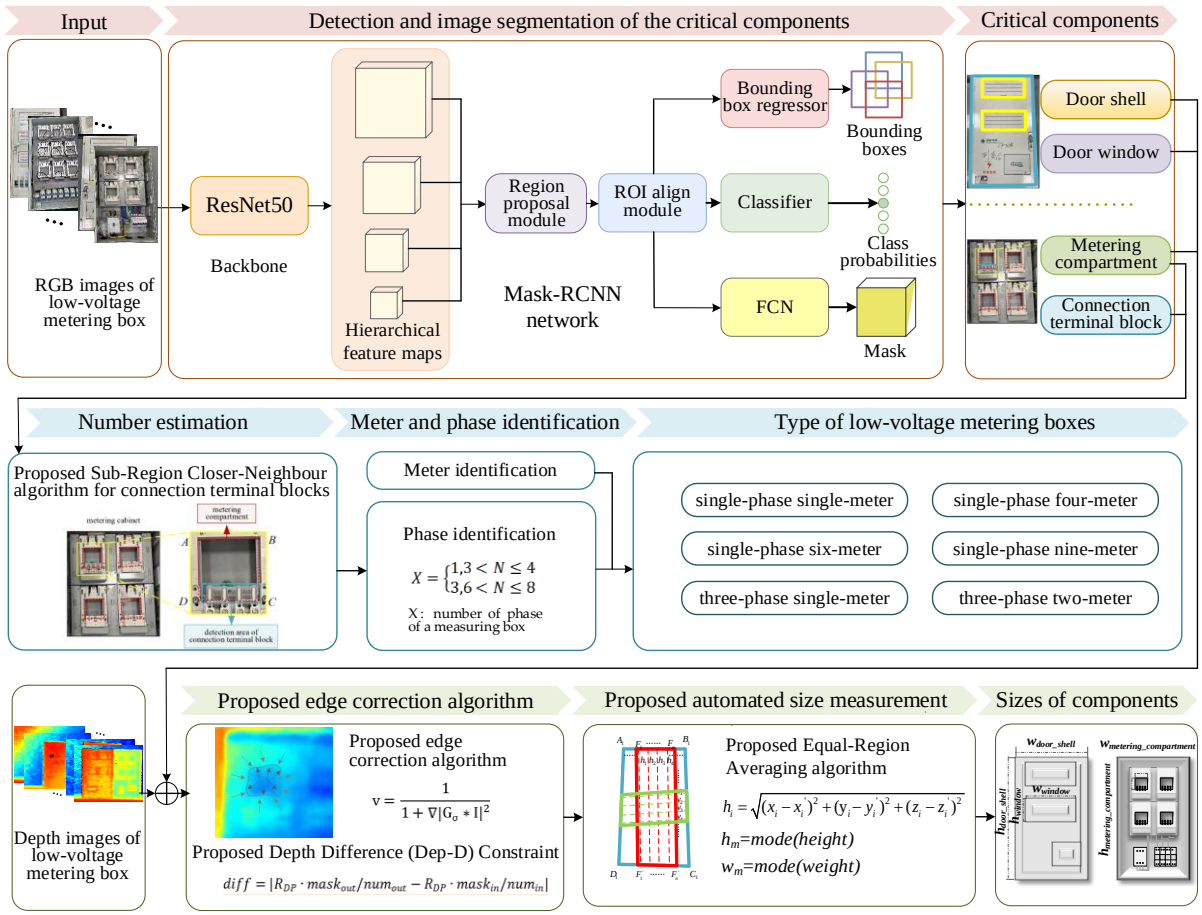

Fig. 2. Flow chart of automated type identification and size measurement for low-voltage metering boxes based on RGB-D images.

The appearance and structure inspection are important in the production, transportation, installation, operation and maintenance of low-voltage metering boxes. The automated inspection could enhance the efficiency of industries, and save labor forces.

In this work, a system for the automated type identification and size measurement of the low-voltage metering boxes is proposed. The overall process flowchart of the system algorithm is shown in Fig. 2.

The critical components of low-voltage metering boxes are detected and segmented by using Mask-RCNN network [27]. The numbers of metering compartments and connection terminal blocks are detected automatically based on the proposed methods. Then according to the phase and number of meters, the type of low-voltage metering boxes is identified. For the segmented contour of the door shell, door window, and metering compartment, the edge correction algorithm is presented to refine the border of the components in the depth images. The Equal-Region Averaging algorithm is proposed to measure the size of these components in the metering boxes.

A. *Detection and Image Segmentation of the Critical Components*

The automated detection and segmentation of the critical components of the metering boxes in the RGB images is the foundation for the automated type identification and size measurement. By combining the detection results and segmented masks, the numbers of metering compartments and connection terminal blocks in the cabinet can be calculated, which are key for the classification of various types of low-voltage metering boxes.

The size inspection of the critical components is the basis for the production, transportation, installation, and maintenance of the metering boxes. All the parts must comply with the requirements in the design drawings and the relative specifications and standards. By combining the detection and segmentation results with the depth information, the sizes of the critical components can be calculated.

Mask-RCNN is a powerful object detection and instance segmentation network. It extends the multi-task network structure based on Faster R-CNN, which, in addition to learning bounding boxes and class labels in a multi-task fashion, adds a third branch for predicting object masks. This method combines the advantages of both object detection and semantic segmentation, achieving accurate and detailed object location and precise segmentation in complex scenes. The Mask-RCNN architecture consists of a backbone convolutional neural network, a region proposal network used to generate object region proposals, and a network branch for predicting object masks. The architecture of the Mask-RCNN network is illustrated in Fig. 3.

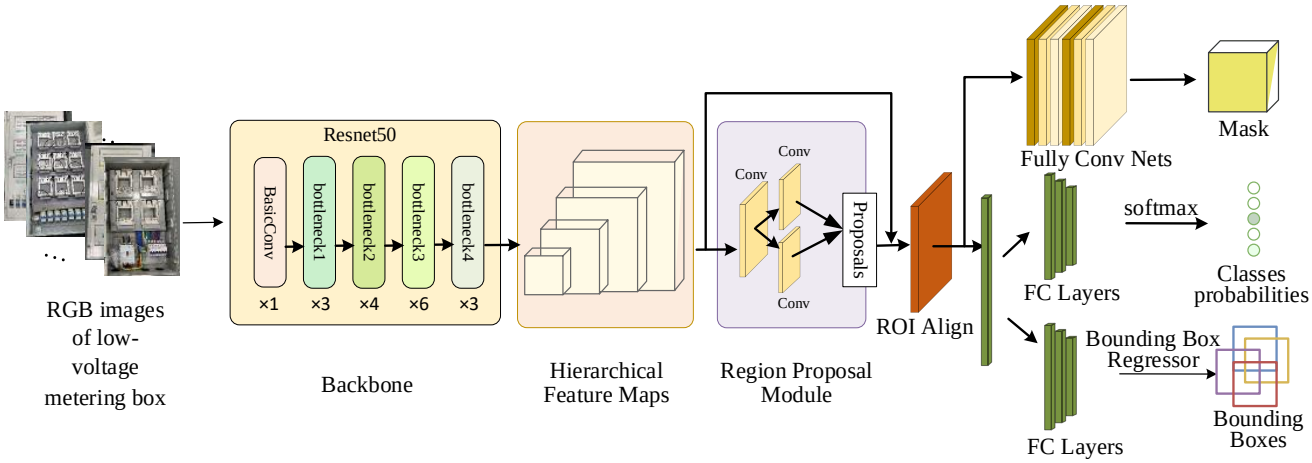

Fig. 3. The architecture of the Mask-RCNN network.

The backbone network is utilized for hierarchical feature extraction from images, while the region proposal network is employed for object detection and generation of candidate regions. The extraction of candidate regions is essentially bounding box regression. For an external bounding box G of the target, its four vertex coordinates are denoted by (G_x, G_y, G_w, G_h). For the proposed initial rectangular region P, its four vertices are represented by (P_x, P_y, P_w, P_h).P Obtaining the target bounding box means finding a mapping f based on the given (P_x, P_y, P_w, P_h). Given a set of parameters W learned through a network for the given input feature vector X, it can be mapped to the target feature vector Y, i.e., $Y \approx WX$, that is:

$$f(P_x, P_y, P_w, P_h) = (\hat{G}_x, \hat{G}_y, \hat{G}_w, \hat{G}_h) \quad (1)$$

$$(\hat{G}_x, \hat{G}_y, \hat{G}_w, \hat{G}_h) \approx (G_x, G_y, G_w, G_h) \quad (2)$$

where the $(\hat{G}_x, \hat{G}_y, \hat{G}_w, \hat{G}_h)$ is derived by the translations and scale transformations depicted in (5) and (6).

The goal of bounding box regression learning is to solve the four transformations $t = (t_x, t_y, t_w, t_h)$, where (t_x, t_y) represents the translation transformation and (t_w, t_h) represents the scale scaling. The formulas are shown in (3) and (4).

$$t_x = P_w d_x(P),\ t_y = P_h d_y(P) \quad (3)$$

$$t_w = \exp d_w(P),\ t_h = \exp d_h(P) \quad (4)$$

$$\hat{G}_x = t_x + P_x$$
$$\hat{G}_x = t_y + P_x \quad (5)$$

$$\hat{G}_w = P_w t_w$$
$$\hat{G}_h = P_h t_h \quad (6)$$

Based on the above formulas, it can be concluded that the objective function for bounding box regression is:

$$d_*(P) = w_*^T \delta(P) \quad (7)$$

where $* = (x, y, w, h)$ and $\delta(P)$ is the input target parameter, w_* is the parameter to be determined, and $d_*(P)$ is the predicted value. By introducing the loss function

$$loss = \sum_{i=1}^{N} (t_*^i - w_*^T \delta(P^i))^2 \quad (8)$$

the optimization objective of the function is:

$$w_* = \arg\min_{w_*} (t_*^i - w_*^T \delta(P^i))^2 + \lambda \|w_*\|^2 \quad (9)$$

By following the aforementioned bounding box regression process, the desired target bounding boxes are obtained. Mask-RCNN has high detection and segmentation accuracies and generalization abilities, making it suitable for object detection and instance segmentation tasks in complex scenes.

B. Automated Type Identification Algorithm for the Low-voltage Metering Boxes

The type of low-voltage metering boxes can be determined by the number of connection terminal blocks and metering compartments. In this section, the number of connection terminal blocks is estimated by using the proposed Sub-Region Closer-Neighbor algorithm. Then, the number of metering compartments is added, and the type of a metering box can be determined.

1) Proposed Sub-Region Closer-Neighbor algorithm for the number estimation of connection terminal blocks: The single-phase metering box is typically connected to a live line and a neutral line in order to measure the amount of electricity flowing into a building or property. For each meter in the metering cabinet, there are two connection terminal blocks for the incoming and outgoing of live lines, and another two connection terminal blocks for the incoming and outgoing of neutral lines. Therefore, there are four connection terminal blocks in a single-phase low-voltage metering box.

Three-phase meter boxes are connected by two live wires and one neutral wire [28]. Inside a three-phase metering box, a single electric meter requires six terminal connection blocks for the live wires to enter and exit and two terminal connection

blocks for the neutral wire to enter and exit, so the number of terminal connection blocks for a single electric meter inside a three-phase metering box is eight.

Due to the complex structure of the metering boxes, as well as the influence of lighting and shooting angle, there are differences in brightness and shading of the connection terminal blocks on the image. This leads to errors in the automated segmentation algorithm. Moreover, the occlusion of wire or baffle plate in front of the connection terminal blocks will results in incomplete or miss segmentation.

In this paper, a quantity estimation algorithm for connection terminal blocks is proposed, to determine whether the metering box is single-phase or three-phase. The connection terminal blocks are located below the metering compartment, as shown in Fig. 4. Fig. 4 shows the inner surface of a low-voltage measuring box, the red dashed box shows the metering compartment region segmented based on the Mask-RCNN network. The four corners of each metering compartment are labeled as A, B, C and D. The connection terminal block region is defined as a quadrilateral I, with a length of $max(L_{AB}, L_{CD})$ and a width of$max(\frac{1}{2}L_{BC}, \frac{1}{2}L_{AD})$, which is symmetric with respect to the corner C and corner D connection line.

In the defined detection region, if there are connection terminal blocks inside, the number of connected domains is calculated, and set to N.

With the number of phase of a low-voltage measuring box denoted as X, the phase discrimination of the low-voltage metering box is shown as follows:

$$X = \begin{cases} 1, 3 < N \leq 4 \\ 3, 6 < N \leq 8 \end{cases} \quad (10)$$

When the average number of connection terminal blocks in a metering box is close to four, this low-voltage metering box is a single-phase metering box; when the average number of low-voltage metering box is close to eight, the low-voltage measuring box is a three-phase metering box.

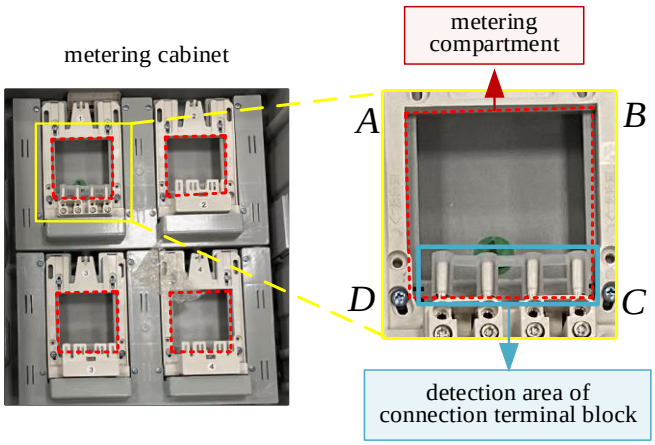

Fig. 4. Schematic diagram of connection terminal block detection region.

Under an occlusive situation, the connection terminal blocks might be incompletely segmented. However, the proposed number estimation algorithm could still detect the number of the connection terminal blocks, and determine the phase of the metering box.

2) Number estimation of metering compartment: Based on the segmented results of the metering compartments, the number of metering compartments is estimated by counting the number of metering compartment regions. The metering compartment might be incompletely segmented. Under this situation, the count in the region is still taken. The number of metering compartments is set as *M*, *M=1,2,…,k*.

C. Edge Correction Algorithm Based on the Depth Difference (Dep-D) Constraint

Due to the influences of factors such as the shooting angle, illumination and shooting time of the depth camera, there may be errors in the edge of R_0. To correct the edge of R_0 and reduce the impact on the accuracy of subsequent size measurement, an edge correction algorithm based on the depth difference constraint is proposed. The algorithm pseudocode is as follows:

Algorithm 1 Edge correction algorithm based on the Dep-D Constraint

Input:
1. I(x, y): The depth image R_{DP}.
2. E_0(x, y): The edge of R_0.

Output:
3. E_{out}(x, y): The corrected edge of R_0.
4. C_i(x, y) ← E_0(x, y) // The initial contour
5. **repeat**
6. C_i.normal ← normalize(C_i(x, y)) // The direction of contour movement
7. v ← $1/(1 + \nabla|G_\sigma * I|^2)$ // The speed of contour movement
8. C_i(x, y) ← movement(C_i, C_i.normal, v) // Move the contour in the specified direction and speed
9. $mask_{out}$, $mask_{in}$, num_{out}, num_{in}← template(C_i) // Establish templates based on the shape and size of C_i
10. $diff_i \leftarrow |I \cdot mask_{out}/num_{out} - I \cdot mask_{in}/num_{in}|$ // The constraint condition
11. diff.append($diff_i$) // Store the results of each loop into an array
12. **until** $diff_i$ = max(diff)

1) Steps of the proposed edge correction algorithm: The steps of the proposed edge correction algorithm are as follows:

Step 1: Set the edge of R_0 (E_0) as the initial contour.

Step 2: Move each point on the contour to make it closer to the true edge. To improve the correction speed, the direction of contour movement is the normal direction of the contour curve where the contour is located. The speed of contour movement is controlled by the depth gradient corresponding to the point, which is calculated as follows:

$$v = \frac{1}{1 + \nabla|G_\sigma * I|^2} \quad (11)$$

where *v* is the calculated speed of contour movement, G_σ represents the Gaussian kernel, which smooths the image, and *I* denotes the depth image R_{DP}. If the gradient is small, it indicates that the point is far from the real edge, and the motion speed is increased; otherwise, the motion speed is decreased.

Step 3: After all points in the contour are changed, the constraint condition for the contour is calculated. Steps 2 and step 3 are repeated until the constraint conditions are met.

2) Constraint condition based on the proposed outer and inner templates: In this work, two structure templates are proposed to build the constraint condition. The two structure templates are illustrated in Fig. 5.

Because of the hollow region in the middle of the metering compartment where the electricity meter is located, there is a significant depth difference inside and outside the edge of the metering compartment. As shown in Fig. 5, an outer template $mask_{out}$ and an inner template $mask_{in}$ are introduced to determine whether the current contour is the edge of the measuring box. The size and the shape of $mask_{out}$ and $mask_{in}$ are consistent with the current contour. As shown in Fig. 5, in the $mask_{out}$, the outermost two layers of the outer template are all assigned the valued of 1, and the values of the remaining layers are all set to 0. In the $mask_{in}$, the outermost two layers of the outer template are all assigned values of 0, and the values of the remaining layers are all set to 1. The two structure templates with the metering compartments in depth image R_{DP} are combined, and the distance difference between the edge and the interior of the bounding box in the depth camera can be calculated. The distance difference can be expressed as follows:

$$diff = \left| I \cdot \frac{mask_{out}}{num_{out}} - I \cdot \frac{mask_{in}}{num_{in}} \right| \qquad (12)$$

where num_{out} and num_{in} represent the number of elements with values of 1 in the $mask_{out}$ and $mask_{in}$, respectively.

When the contour moves to the true edge, due to the difference in the depth values between the inner and outer edges, the *diff* value will reach its maximum value (the red point in Fig. 6). In this work, when the *diff* starts to decrease, it is considered to meet the constraint condition and the iterations stop. The contour obtained in this iteration is the corrected edge.

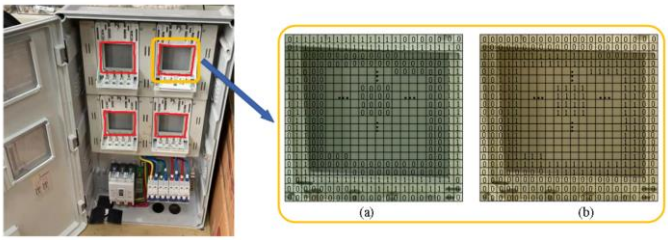

Fig. 5. The proposed structure templates: (a) outer template and (b) inner template

D. Automated Size Measurement based on the Proposed Equal-Region Averaging Algorithm

Due to the errors caused by the infrared pattern projected by the depth camera during the imaging process, as well as the errors caused by the stereo matching algorithm, some pixels' depth information is missing or deviating in the depth image [29]. To obtain more accurate depth-channel information and realize automated size measurement, the Equal-Region Averaging algorithm is proposed in this work. The steps are as follows:

Step 1: Calculate the bounding box of the segmented region. The segmented components are the door shell, window and metering compartment.

Step 2: Obtain the four corners of the bounding box. Set a_i *(i=1,2,3,4)* as the distance parameters between each corner and all the points on the segmented region.

Step 3: Define four pseudo-corners as the points on the segmented contour, which have the minimal distances to their corresponding corners. The pseudo-corners cut the contour into four segments.

Step 4: For each segment, find the midpoint of each segment, and take the midpoint as the center to obtain a detection area with a length of one-quarter of the side length. In Fig. 7, the red box line represents the length detection range of the door shell, window or metering compartment. And the green box line represents the width detection range of the component.

In the defined detection region, the corresponding pixel points on the opposite sides are connected. The length of each line can be calculated as:

$$h_i = \sqrt{(x_i - x_i^{'})^2 + (y_i - y_i^{'})^2 + (z_i - z_i^{'})^2} \qquad (13)$$

where the 3D coordinate values of the corresponding pixel pair are $F_i(x_i, y_i, z_i)$ and $F_i^{'}(x_i^{'}, y_i^{'}, z_i^{'})$.

The vector of the heights is:

$$height = [h_1, h_2, h_3 \ldots . h_i] \qquad (14)$$

and the vector of widths is:

$$width = [w_1, w_2, w_3 \ldots . w_i] \qquad (15)$$

The mode of these two vectors is calculated, and the values h_m and w_m are the height and weight of the component.

$$h_m = mode(height),\ w_m = mode(weight) \qquad (16)$$

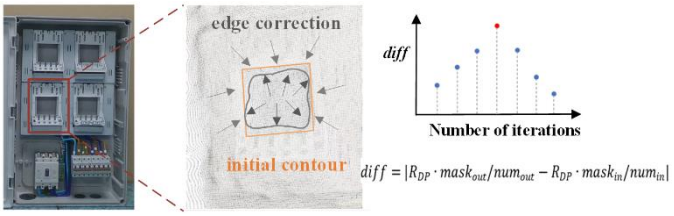

Fig. 6. The proposed edge correction algorithm based on the Depth Difference (Dep-D) Constraint

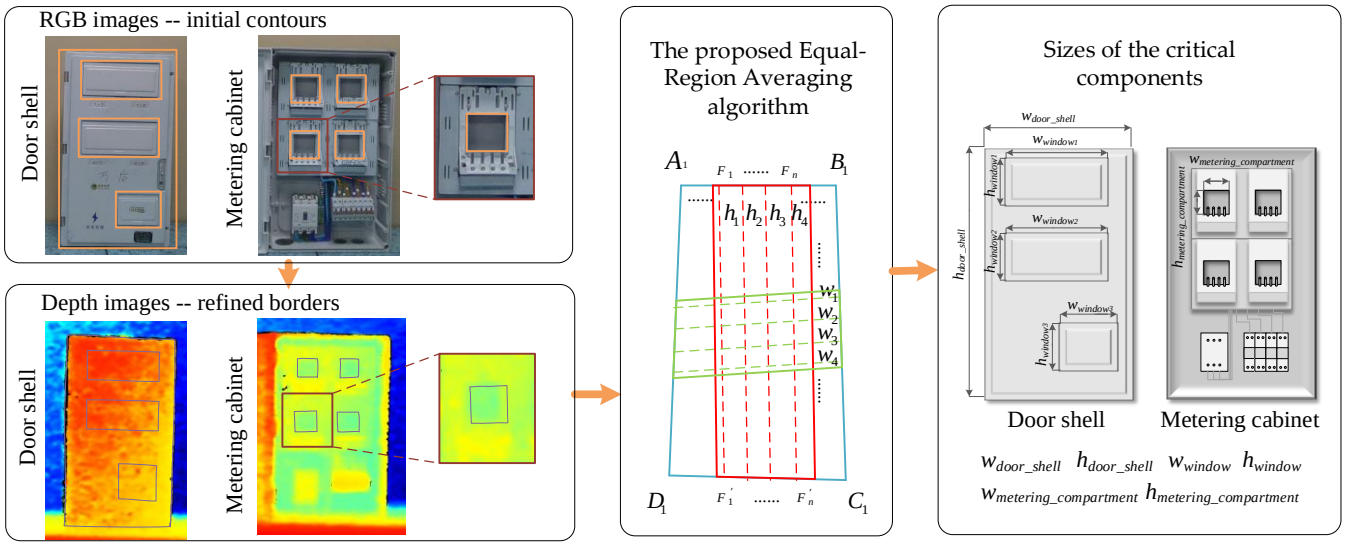

Fig. 7. Schematic diagram of size measurement region of door shell, window and metering compartment.

III. Experimental Results and Analysis

In this work, an automated type identification and size measurement method is proposed for the low-voltage metering boxes, which are among the most critical pieces of equipment in a power system.

A. RGB-D Image Data of Low-voltage Metering Boxes

Six types of low-voltage metering boxes are collected in this work, namely single-phase single-meter, single-phase four-meter, single-phase six-meter, single-phase nine-meter, three-phase single-meter, and three-phase two-meter low-voltage metering boxes. Table I shows the diagrams of the outer shell and the inner surfaces of these six types of low-voltage metering boxes.

The RGB-D images are captured using the Intel RealSense D415 depth cameras developed by Intel Corporation. The image resolution is 1280*720. A total of 732 images are collected as experimental data.

B. Experimental Results of Type Identification for Low-voltage Metering Box

In the RGB channel, the metering compartment and connection terminal block are segmented by using the Mask-RCNN network first. Then, the number of connection terminal blocks is estimated by using the proposed Sub-Region Closer-Neighbor algorithm. Combined with the depth information, the contours of the metering compartments are re-fined. The number of metering compartments is estimated, by counting the connected do-main of metering compartment regions. Finally, the type of low-voltage metering box is identified by using the number of metering compartments and connection terminal blocks.

1) Experimental results of type identification for low-voltage metering box: In this work, six types of low-voltage metering boxes are classified. Table II shows the detection accuracies for these six types of low-voltage metering boxes.

From Table II, it can be seen that average detection accuracies of the proposed type identification method for the low-voltage metering boxes reach up to 94.8%. The detection accuracies for six types of low-voltage metering box range from 92.3% to 96.8%.

TABLE I. Six Types of Low-Voltage Metering Boxes

Single-phase single-meter		Single-phase four-meter	
Outer shell	**Cabinet**	**Outer shell**	**Cabinet**
			
Single-phase six-meter		**Single-phase nine-meter**	
Outer shell	**Cabinet**	**Outer shell**	**Cabinet**
			
Three-phase single-meter		**Three-phase two-meter**	
Outer shell	**Cabinet**	**Outer shell**	**Cabinet**
			

TABLE II. DETECTION ACCURACIES OF DIFFERENT TYPES OF LOW-VOLTAGE METERING BOXES

Type	Detection accuracy	Average accuracy
Single-phase single-meter	92.3%	94.8%
Single-phase four-meter	96.8%	
Single-phase six-meter	93.6%	
Single-phase nine-meter	95.7%	
Three-phase single-meter	92.5%	
Three-phase two-meter	93.1%	

The recognition accuracies of single-phase single-meter and single-phase nine-meter metering boxes are lower than those of the other types, mainly due to the misdetection of the number of connection terminal blocks. The counting accuracy of the connection terminal blocks is reduced due to illumination, occlusion, and other problems. In particular, the baffle plate in front of the connection terminal blocks significantly affects the segmentation accuracy. In this work, the Sub-Region Closer-Neighbor algorithm is proposed to reduce the influence of occlusion. The proposed method could increase the recognition accuracy even if the connection terminal blocks are incompletely segmented. Moreover, even if part of the connection terminal block is misdetected, the proposed method could still reduce the detection error, by inducing the (8). The distance between the detected number and the standard number (4 or 8) is calculated. The final number of connection terminal blocks is the number with the smallest distance from the standard number. If the connection terminal blocks are fully occluded, misjudgment of the phase could occur.

2) Experimental results of critical components segmentation and number detection method: To identify the types of low-voltage metering boxes, the critical components in the metering box are segmented first. Then, the Sub-Region Closer-Neighbor algorithm is proposed to estimate the number of terminal blocks. The defined Depth Difference (Dep-D) Constraint is used in the edge correction algorithm, to refine the contour of the metering compartments. The number of metering compartments is estimated based on the segmentation results. Table III lists the results of the automated segmentation and counting methods for metering compartments and connection terminal blocks.

As shown in Table III, the Intersection over Union (IoU) values for the segmentation of the connection terminal block, rang from 75.5% to 89.6%.

The precision of segmentation for the connection terminal blocks is affected by many factors. The color of the connection terminal block is gray, which is close to color of the metering cabinet panel. The location of connection terminal block is below the metering compartment. Most of the time, there is a baffle plate set in front of the connection terminal block, in order to protect the wires. The connection terminal block could only be seen in the gap of plate stripes. Sometimes, the wires can occlude the connection terminal block as well. Fig. 8 illustrates the situations which affect the detection accuracy of connection terminal blocks.

TABLE III. RESULTS OF AUTOMATED SEGMENTATION AND COUNTING METHODS FOR CONNECTION TERMINAL BLOCK AND METERING COMPARTMENT

Type of metering box	Component	IoU	Number counting	Type identification
Single-phase single-meter	CTB	78.6%	94.7%	92.3%
	MC	93.3%	100%	
Single-phase four-meter	CTB	75.5%	88.9%	96.8%
	MC	90.2%	99.5%	
Single-phase six-meter	CTB	80.5%	90.5%	93.6%
	MC	94.5%	99.7%	
Single-phase nine-meter	CTB	83.6%	90.0%	95.7%
	MC	90.6%	98.7%	
Three-phase single-meter	CTB	86.4%	93.8%	92.5%
	MC	90.6%	98.6%	
Three-phase two-meter	CTB	89.6%	90.6%	93.1%
	MC	94.9%	97.5%	

Component CTB: Connection Terminal Block, Component MC: Metering Compartment

Due to the occlusion, illumination, and shooting angle, the connection terminal blocks could be mis-segmented, or incompletely segmented. Although the IoU of the segmentation of the connection terminal block is lower than 89.6%, the accuracy of the number counting ranges from 88.9% to 94.7%, for the proposed Sub-Region Closer-Neighbor algorithm.

The segmentation of the metering compartments is implemented by Mask-RCNN network in the RGB images. The shape and structure features of the metering compartment are identical in the metering cabinet. Sometimes, occlusion or incomplete image acquisition occur due to the different shooting angles. These will influence the segmentation accuracy. In spite of these influences, the number counting accuracy of the metering compartment is still above 97.5%. In the number counting algorithm, as long as the object is classified as the metering compartment, the number of metering compartments is counted. This will reduce the influence of occlusion. Based on the critical component segmentation and number counting, the type of metering box is identified. The detection accuracy is above 92.3%.

C. Experimental Results of Automated Size Measurement for Low-voltage Metering Box

The size and structural design of the low-voltage metering boxes should fully con-sider the layout of the components and the functional requirements of the appearance.

According to Enterprise Standard Q/GDW 11008-2013 "Technical Specification for Low-Voltage Metering Box" [23], released by the State Grid Electric Power Co., Ltd., the component sizes of the low-voltage metering boxes should meet the enterprise standard, and the size errors should be within a certain range. Size inspection is required over the whole life of the metering box, including the manufacture, transportation, on-site installation, and daily usage.

1) Quantitative metrics for size measurement: In this work, an automated size measurement method is presented, to automatically detect the size of the door shell, door window, and metering compartment in the cabinet.

(a) Partially occlusion by wire

(b) Differences in brightness and shading

(c) Partial occlusion by baffle plate

(d) Complete occlusion by baffle palate

Fig. 8. The situations which affect the detection accuracy of connection terminal blocks.

The critical components are segmented by using the Mask-RCNN network in the RBG images. The edge correction algorithm based on the Depth Difference (Dep-D) Constraint is proposed in this work. The refinement algorithm uses the information in the depth-channel. Based on the refined contours of the components, the size is measured based on the proposed Equal-Region Averaging algorithm.

The precision of the proposed size measurement algorithm is indicated by the following metric:

$$p = \begin{cases} ture, error < \alpha \\ false, error \geq \alpha \end{cases} \quad (17)$$

If the average calculation error is within α, then this measurement result is correct.

2) Experimental results for size measurement: In the Enterprise Standard Q/GDW 11008-2013 "Technical Specification for Low-Voltage Metering Box", it is stipulated that the size error of the metering box shell should not exceed 5mm. This work set the α as 5mm, 4mm, 3mm, and 2mm. The experimental results are shown in Table IV.

As shown in Table IV, the accuracy of the size measurement is 92.6%, when α is set to 5mm. When the α is set to 2mm, the detection accuracy is still above 85%.

In this work, three critical components need to be measured, which are the door shell, door window, and the metering compartment in the cabinet. The regions of these components are segmented in the RGB images using the Mask-RCNN network.

For the Intel Real Sense depth camera, the RGB image is aligned with that in the depth image. The spatial location information of the object is acquired in the depth channel. The Intel RealSense D415 camera is used to capture depth data by projecting an infrared laser pattern onto the scene, and measuring how it is reflected back to the camera's sensors.

TABLE IV. RESULTS OF AUTOMATED SIZE MEASUREMENT FOR THE CRITICAL COMPONENTS OF LOW-VOLTAGE METERING BOX (%)

Type of metering box	Component	Measuring Accuracy			
		α_1	α_2	α_3	α_4
Single-phase single-meter	DS	94.3	93.5	90.6	90.3
	DW	90.1	88.4	86.4	85.1
	MC	94.3	91.5	89.6	87.3
Single-phase four-meter	DS	93.2	92.7	91.2	90.9
	DW	93.7	92.3	91.9	91.2
	MC	91.4	91.5	90.3	89.4
Single-phase six-meter	DS	95.2	92.5	90.6	89.5
	DW	94.2	92.7	91.3	89.4
	MC	90.5	89.3	88.5	87.5
Single-phase nine-meter	DS	94.3	92.5	91.6	90.1
	DW	92.2	91.8	89.3	87.6
	MC	95.3	92.3	90.5	88.1
Three-phase single-meter	DS	93.3	91.5	89.6	88.3
	DW	93.4	91.5	89.3	85.6
	MC	94.8	92.5	92.5	86.7
Three-phase two-meter	DS	93.6	92.5	91.8	89.9
	DW	91.5	90.3	89.1	88.3
	MC	93.1	92.5	90.2	89.5
Average measuring accuracy: 92.6%（α_1=5mm）, 91.8%（α_1=4mm）, 90.4%（α_1=3mm）, 87.5%（α_1=2mm）					

Component DS: Door Shell, Component DW: Door Window, Component MC: Metering Compartment

The segmented contours in the RGB images are used as the initial borders in the depth images. Then, the proposed edge correction algorithm based on the Depth Difference (Dep-D) Constraint is applied. This border refinement algorithm considers the depth difference between the outside and inside of the border. The actual contour is estimated after iteration, by balancing the gradient on the border.

D. Comparison with State-of-the-art Methods

In this work, a method is proposed to classify six types of low-voltage metering boxes. In this section, the proposed method is compared with state-of-the-art methods: the VGG [30], YOLO [31-32], EfficientDet [33], and ResNet [34-35] networks.

The VGG network comprises of different variants of convolutional neural networks, stacking multiple convolutional layers with small-sized convolution filters along with max-pooling layers [30]. The YOLO network uses a single convolutional neural network to predict both object class probabilities and bounding boxes directly from full images in one go [32]. The EfficientDet network applies a compound scaling approach to optimize both model architecture and input resolution [33]. The ResNet network solves the problem of vanishing gradients in the deep neural networks by using residual connections that allow the network to pass information directly from the input to the output [34]. All of these above networks have been widely used on various image classification tasks. Table V shows the comparison results.

TABLE V. RESULTS OF AUTOMATED IDENTIFICATION OF SIX TYPES OF LOW-VOLTAGE METERING BOXES (%)

Type of metering box	VGG [30]	YOLO [31-32]	EfficientDet [33]	ResNet [34-35]	Ours
Single-phase single-meter	73.4	69.3	75.2	80.4%	**92.3**
Single-phase four-meter	81.4	89.2	83.2	90.2%	**96.8**
Single-phase six-meter	80.5	85.2	79.3	82.9%	**93.6**
Single-phase nine-meter	85.7	90.1	89.2	91.4%	**95.7**
Three-phase single-meter	71.5	73.5	78.9	75.2%	**92.5**
Three-phase two-meter	87.4	86.4	92.5	84.5	**93.1**

As shown in Table V, our proposed type identification method achieves the highest classification accuracy. The classification accuracies for six types of low-voltage metering box are above 92.3%.

The state-of-the-art networks achieve the classification accuracies ranging from 69.3% to 92.5%. For these networks, the metering box images with labels are input to the net-works, to implement a six-type multi-class classification task. The dataset tested in this work includes a total of 732 images, which could lead to overfitting, where the model becomes too specialized to the training data.

Although the metering compartments are notable features in the images, the type of the metering boxes need to be decided by the number of metering compartments and connection terminal blocks at the same time. The detection of connection terminal blocks is more difficult, due to their shapes, sizes, colors and locations. The misdetection of connection terminal blocks could lead to the wrong classification of metering box types.

Our proposed method considers many factors in the type identification task. The proposed Sub-Region Closer-Neighbor algorithm could count the number of connection terminal blocks in scenarios with complex illumination and occlusion.

IV. CONCLUSIONS

The low-voltage metering box is one of the most crucial pieces of equipment in a power system network. In this work, a metering box identification system based on the computer vision techniques is studied to realize automated detection of the appearances and structures of metering boxes. An automated type identification and size measurement method for the low-voltage metering box is proposed.

The following are the main steps of this proposed method. The critical components, including the door shell and window, connection terminal block, and metering compartment in the cabinet, are segmented first using the Mask-RCNN network. Then the proposed Sub-Region Closer-Neighbor algorithm is used to estimate the number of connection terminal blocks. Combined with the number of metering compartments, the type of metering box is classified. To refine the borders of the metering box components, an edge correction algorithm based on the Depth Difference (Dep-D) Constraint is presented. Finally, the automated size measurement is implemented based on the proposed Equal-Region Averaging algorithm.

The primary contributions of this study are as follows. Firstly, the proposed Sub-Region Closer-Neighbour algorithm enables a more precise estimation of the number of connection terminal blocks, which is an essential parameter for the type identification of a metering box. This results in higher classification accuracies when compared to existing deep learning methods [30-35]. Secondly, to obtain more accurate size measurements, an edge correction algorithm is proposed. Then the automated size measurement is implemented based on the proposed Equal-Region Averaging algorithm.

There are two primary challenges in this study. The first is the occlusion of the connection terminal block, which leads to incorrect classification of the metering box type. The second challenge is the limitations of the depth camera, which introduces errors in size measurement. While this study proposes solutions to overcome these challenges, there is a need for further work to enhance detection and measurement accuracy.

One drawback of this article is that it involves numerous calculation steps, making the calculations complicated. Furthermore, in order to capture both segmentation and depth information, the system requires the processing of both RGB and depth images. In future research, it may be worthwhile to explore algorithms that can accomplish automated inspection using depth-images exclusively.

In the future, the improvement of automation level is a development trend in the power system industry. Compared with manual inspection, which can be time-consuming and labor-intensive, the integration of artificial intelligence technology in this field can significantly reduce costs, enhance overall efficiency and optimize resource utilization.

REFERENCES

[1] Wei, J.K.; Yuan, J.F.; Wang, P.; Hong, X.T.; Luo, F. The “Five preventions” Improvement of the Outdoor Low-voltage Metering Box[J]. Mechanical and Electrical Information, 2018(03): 68-69. DOI: 10.19514/j.cnki.cn32-1628/tm.2018.03.037.

[2] Huang, F.; Shen, H.; Zhen, H.H.; Yu, L.; Zhang, J.H.; Han, D.J. Condition Assessment of Low Voltage Metering Box Based on AHP-gray Fixed Weight Clustering[J]. Electrical Measurement & Instrumentation, 2019,56(03): 64-69. DOI: 10.19753/j.issn1001-1390.2019.03.011.

[3] Artale, G.; Cataliotti, A.; Cosentino, V.; Di Cara, D.; Fiorelli, R.; Guaiana, S.; Panzavecchia, N.; Tinè, G. A new PLC-based smart metering architecture for medium/low voltage grids: Feasibility and experimental characterization. Measurement 2018, 129, 479-488, doi: 10.1016/j.measurement.2018.07.070.

[4] Li, H.; Liang, W.; Liang, Y.; Li, Z.; Wang, G. Topology identification method for residential areas in low-voltage distribution networks based on unsupervised learning and graph theory. Electr. Pow. Syst. Res. 2023, 215, 108969, doi: 10.1016/j.epsr.2022.108969.

[5] Su, C.; Lee, W.; Wen, C. Electricity theft detection in low voltage networks with smart meters using state estimation. In 2016 IEEE International Conference on Industrial Technology (ICIT), 2016-01-01 2016; pp. 493-498.

[6] Lukman, F.S.; Dharmawan, H.E.S.; Ramadhani, K. Portable Smart Energy Meter for Low Voltage Customer of Power 53 -197 KVA. In 2022 International Conference on Technology and Policy in Energy and Electric Power (ICT-PEP), 2022, pp. 60-64.

[7] Zhu, Y.; Chen, L.; Fu, Y.; Zhang, H.; Zhao, G. Design and Engineering Application of Low Voltage Power Grid. In 2022 5th International Conference on Power and Energy Applications (ICPEA), 2022, pp. 410-413.

[8] Zheng, A.; Yuan, X.; Shang, H.; Xiong, S.; Cheng, D. Evaluation of Aging Properties of Nonmetal Low Voltage Metering Box Shells under Typical Environment. In 2020 International Conference on Artificial Intelligence and Electromechanical Automation (AIEA), 2020, pp. 827-831.

[9] Jiang, Y.; Song, X.; Lin, H.; Zhao, Y.; Qiu, K.; Yang, C.; Dong, S. Topology Automatic Identification Method for Low-Voltage Stations Based on Line Impedance Analysis. IOP Conference Series: Earth and Environmental Science 2021, 687, 12116, doi: 10.1088/1755-1315/687/1/012116.

[10] Xu, C.; Lei, Y.; Zou, Y. A Method of Low Voltage Topology Identification. In 2020 IEEE Conference on Telecommunications, Optics and Computer Science (TOCS), 2020, pp. 318-323.

[11] Nainar, K.; Iov, F. Smart Meter Measurement-Based State Estimation for Monitoring of Low-Voltage Distribution Grids. Energies 2020, 13, 5367, doi: 10.3390/en13205367.

[12] Shuai, G.; Qiong, S.W.; Ji, L.; Wen, B.Z.; Rui, L.; Qiang, W.; Fei, M.H. Design of Intelligent Low Voltage Station System Based on Edge Calculation. Journal of Physics: Conference Series 2021, 1972, 12050, doi: 10.1088/1742-6596/1972/1/012050.

[13] Wang, Y.; Hou, H.J.; Hua, J.; Li, Y.H.; Tu,Z.W. Design and Application of Intelligent Detection Management System for Low-voltage Metering Box[J]. Electrical Measurement & Instrumentation, 2020,57(08): 147-152. DOI: 10.19753/j.issn1001-1390.2020.08.023.

[14] Shen, H.; Cao, Y.; Lei, Y.; Zhen, H.; Zhang, J.; Han, D. Main Fault Types and Classification Methods of Metering Box[C]//IOP Conference Series: Materials Science and Engineering. IOP Publishing, 2018, 394(4): 42096-42097.

[15] Xu, J.Y. Design of Monitor Terminal for Image Data in Electric Power Metering Device[J]. Information Technology, 2014(06): 184-186. DOI: 10.13274/j.cnki.hdzj.2014.06.014.

[16] Weng, D.B.; Chen, R.B.; Dou, X.W. Design of Electric Meter Measuring-box Based on Wireless Image Transmission[J]. Instrumentation Technology, 2012(10): 51-53. DOI: 10.19432/j.cnki.issn1006-2394.2012.10.015.

[17] Wu, X. Measurement of Sizes of Non-contact Screws Based on Visual Recognition Technology[J]. Metrology & Measurement Technique, 2019,46(08): 40-42. DOI: 10.15988/j.cnki.1004-6941.2019.8.011.

[18] Li, B.Z.; Ni, H.Q.; Lin, S.Y.; Meng, X.C. Axial Dimension Detection Method of Corrugated Compensator Based on Image Recognition[J]. Chinese Journal of Engineering Design, 2022,29(01): 10-19. DOI: 10.3785/j.issn.1006-754X.2022.00.012.

[19] Chen, Y.; Bian,G.H.; Yang, P.; Yu, L.P.; Wang, C.Y. Pipe Size Characteristic Parameter Collection and Detection System Based on Image Recognition[J]. Nondestructive Testing, 2022,44(09): 22-27. DOI: 10. 11973 /wsjc202209005.

[20] Chen, W.B. The Dimensional Inspection and Surface Defect Recognition of Injection Molded Products Based on Machine Vision[D]. Master, Huazhong University of Science and Technology, 2015.

[21] Yu, J.J. Human Dimension Recognition System Based on Machine Vision[J]. Light Industry Machinery, 2014,32(03): 60-62. DOI: 10.3969/j.issn.1005-2895.2014.03.015.

[22] Xue, L.J.; Qi, C.K.; Zhang, B.; Zhang, X.Y.; Wu, C.Z. Object Size and Orientation Recognition Based on 3D Point Cloud Euclideam Clustering and RANSAC Boundary Fitting[J]. Machine Design and Research, 2018,34(05): 44-48. DOI: 10.13952/j.cnki.jofmdr.2018.0187.

[23] Liu, B. Research on the Key Technologies for On-site Dimension Measuring of Large Forging Based on Binocular Stereo Vision[D]. Doctor, Yanshan University, 2010.

[24] Luo, C. Research on the size Measurement System for Hot Forging Based on the Image Edge Recognition[D]. Master, Yanshan University, 2017.

[25] Falcone, G. Multiphase Flow Metering Principles. 2009, 54, 33-45, doi: 10.1016/S0376-7361(09)05403-X.

[26] Zhichun, Y.; Yu, S.; Fan, Y.; Yang, L.; Lei, S.; Fangbin, Y. Topology identification method of low voltage distribution network based on data association analysis. In 2020 5th Asia Conference on Power and Electrical Engineering (ACPEE), 2020-01-01 2020; pp. 2226-2230.

[27] He, K.; Gkioxari, G.; Dollar, P.; Girshick, R. Mask r-cnn. In Proceedings of the IEEE international conference on computer vision, 2017, pp. 2961-2969.

[28] Lai, J.; Shen, J.; Zhang, Y.; Zhong, Z.; Liu, G. A Novel Adjustment Strategy for Reducing Three-Phase Unbalance in Low-Voltage Distribution Area. In 2022 12th International Conference on Power and Energy Systems (ICPES), 2022, pp. 89-93.

[29] Tam, A.Y.; So, B.P.; Chan, T.T.; Cheung, A.K.; Wong, D.W.; Cheung, J.C. A Blanket Accommodative Sleep Posture Classification System Using an Infrared Depth Camera: A Deep Learning Approach with Synthetic Augmentation of Blanket Conditions. Sensors-Basel 2021, 21, 5553, doi: 10.3390/s21165553.

[30] Wang, S.; Khan, M.A.; Zhang, Y. VISPNN: VGG-inspired Stochastic Pooling Neural Network[J]. Computers, Materials & Con-tinua, 2022, 70, 3081. DOI: 10.32604/cmc.2022.019447.

[31] Du, J. Understanding of Object Detection Based on CNN Family and YOLO[J]. IOP Publishing, 2018, p.12029. DOI: 10.1088/1742-6596/1004/1/012029.

[32] Diwan, T.; Anirudh, G.; Tembhurne, J.V. Object Detection Using YOLO: Challenges, Architectural Successors, Datasets and Applications[J]. Multimedia Tools and Applications. 2023, 82, 9243-9275. DOI: 10.1007/s11042-022-13644-y.

[33] Tan, M.; Pang, R.; Le, Q.V. Efficientdet: Scalable and Efficient Object Detection[C]//Proceedings of the IEEE/CVF conference on computer vision and pattern recognition. 2020, pp. 10781-10790.

[34] Wu, Z.; Shen, C.; Van Den Hengel, A. Wider or Deeper: Revisiting the Resnet Model for Visual Recognition. Pattern Recognition, 2019, 90: 119-133. DOI: 10.1016/j.patcog.2019.01.006.

[35] Shafiq, M.; Gu, Z. Deep Residual Learning for Image Recognition: A Survey. Applied Sciences, 2022, 12(18): 8972. DOI: 10.3390/app12188972.